Materials Science & Engineering A 625 (2015) 393–402

Contents lists available at ScienceDirect

Materials Science & Engineering A

journal homepage: www.elsevier.com/locate/msea

The ductile to brittle transition behavior in a Zr-based bulk metallic glass

G. Li [a], M.Q. Jiang [b], F. Jiang [a,*], L. He [a], J. Sun [a,*]

[a] State Key Laboratory for Mechanical Behavior of Materials, Xi'an Jiaotong University, Xi'an 710049, China
[b] State Key Laboratory of Nonlinear Mechanics, Institute of Mechanics, Chinese Academy of Sciences, Beijing 100190, China

ARTICLE INFO

Article history:
Received 14 September 2014
Received in revised form
23 November 2014
Accepted 26 November 2014
Available online 5 December 2014

Keywords:
Ductile to brittle transition
Bulk metallic glass
Fracture
Shear band

ABSTRACT

The ductile to brittle transition (DBT) of crystalline metals and alloys has been extensively studied in scientific and engineering fields. However, the DBT of non-crystalline metals and alloys such as bulk metallic glasses (BMGs) remains poorly characterized and understood. Here, the DBT behavior of a Zr-based ($Zr_{52.5}Cu_{17.9}Ni_{14.6}Al_{10}Ti_5$) BMG as a model material was systematically investigated at various temperatures and different free volume states using uniaxial tensile and compression tests. A significant DBT was confirmed by the observations of the transition of macroscopic fracture modes from shear to tension as well as microscopic fracture surface features from micron-scale vein pattern to nano-scale dimples/periodic corrugations. It is revealed that the former is determined by the intrinsic competition between the critical shear and normal stresses, and the latter is due to the competition between ductile shear banding and brittle cracking. Within the framework of the cooperative shear model of shear transition zones (STZs), a DBT map for metallic glasses is proposed in terms of STZ versus tension transition zone (TTZ), depending on free volume, temperature and strain rate.

1. Introduction

Bulk metallic glasses (BMGs) have been regarded as high performance structural materials due to their unique properties, such as high strength and hardness, large elastic strain, good soft magnetic properties, and excellent corrosion resistance [1–3]. Some Zr-, Pt-, Pd-, Ti- and Cu-based BMGs have fracture toughnesses comparable to those of conventional alloys or even higher [4–8]. Recently, a Zr–Cu–Al–Ti BMG with fracture toughness of about 100 MPa $m^{1/2}$ [9] and a new Pd-based BMG with fracture toughness comparable to those of the toughest materials known [10] have also been developed. Moreover, at cryogenic temperatures (e.g., liquid nitrogen temperature, 77 K), some Ti-, Zr- and CuZr-based BMGs could exhibit better plasticity in compression [11–16] and tension [17,18] or comparable fracture toughness [19] compared with those at room temperature (RT). Therefore, although monolithic BMGs usually show almost zero ductility in tension and limited malleability in compression, their advantage of high strength and good fracture toughness still entails their potential applications in space exploration, liquefied gas storage and cooling pipe of experimental thermonuclear reactor at cryogenic temperatures [11,14].

However, ductile to brittle transition (DBT) could occur in metallic glasses from ribbon (mainly Fe-based) [20–23] to BMGs [24–27] as temperature decreasing according to previous researches. For example, the impact toughness of $Zr_{41.2}Ti_{13.8}Cu_{12.5}Ni_{10}Be_{22.5}$ (Vit1) has been found to be closely related to the test temperature and dramatically decreased below a critical temperature, indicating a clear DBT behavior [25]. Our recent results have also shown that the DBT could be achieved in a $Zr_{52.5}Cu_{17.9}Ni_{14.6}Al_{10}Ti_5$ (Vit105) BMG under three-point bending and uniaxial tension through decreasing test temperatures, accompanied by the transition of both microscopic fracture feature and macroscopic fracture mode [26,27]. Additionally, these tough BMGs could be embrittled and suffered a DBT due to the reduction of free volume concentration by annealing at temperatures below the glass transition temperature T_g [28,29], or decreasing cooling rates during casting [30]. The DBT temperature (DBTT) has also been suggested to be sensitive to the free volume concentration in samples [22,26,28]. So far, toughening or embrittling at cryogenic temperatures, especially DBT behavior-related temperatures of BMGs is still under debate [11,18,31,32]. Several factors on DBT of MGs such as free volume [22], Poisson's ratio [33,34], structural relaxation [35,36], normal stress sensitivity [37] have been put forward. In particular, Lewandowski et al. [33,34] have correlated

* Corresponding authors. Tel.: +86 2982668173; fax: +86 2982663453.
E-mail addresses: jiangfeng@mail.xjtu.edu.cn (F. Jiang), junsun@mail.xjtu.edu.cn (J. Sun).

http://dx.doi.org/10.1016/j.msea.2014.11.088
0921-5093/

the fracture energy of a number of different glasses with Poisson's ratio, a good measure of the intrinsic toughness and plasticity of different MGs [38]. And very recently a universal thermodynamic criterion is also proposed for better understanding the intrinsic correlations between fracture toughness and Poisson's ratio [39]. In our previous paper, we had proposed the STZ volume was a key parameter to understand the DBT behavior in fracture of BMGs based on the cooperative shearing model (CSM) proposed by Johnson and Sawmer [40]. In this paper, we selected a Zr-based BMG (Vit105) as a model material and continued to investigate its mechanical properties and fracture behavior at various temperatures and with different free volume states using uniaxial tensile and compression tests. The underlying mechanism of DBT was systematically discussed. A DBT map was constructed based on the STZ volume to describe both ductile and brittle zones, taking into account free volume, temperature and strain rate. This work will be useful to deeply understand the mechanical properties and guide the application of BMGs.

2. Experiments

The master ingots of Vit105 were produced by arc-melting Zr of 99.8% purity and Cu, Ni, Al and Ti of 99.99% purity in a Ti-gettered argon atmosphere. Plates with dimensions of $50 \times 20 \times 1.5$ mm^3 were prepared using the drop casting method for tensile tests [41]. Other plates with dimensions of $4 \times 10 \times 40$ mm^3 were fabricated by the copper-mold suction-casting method for compression tests.

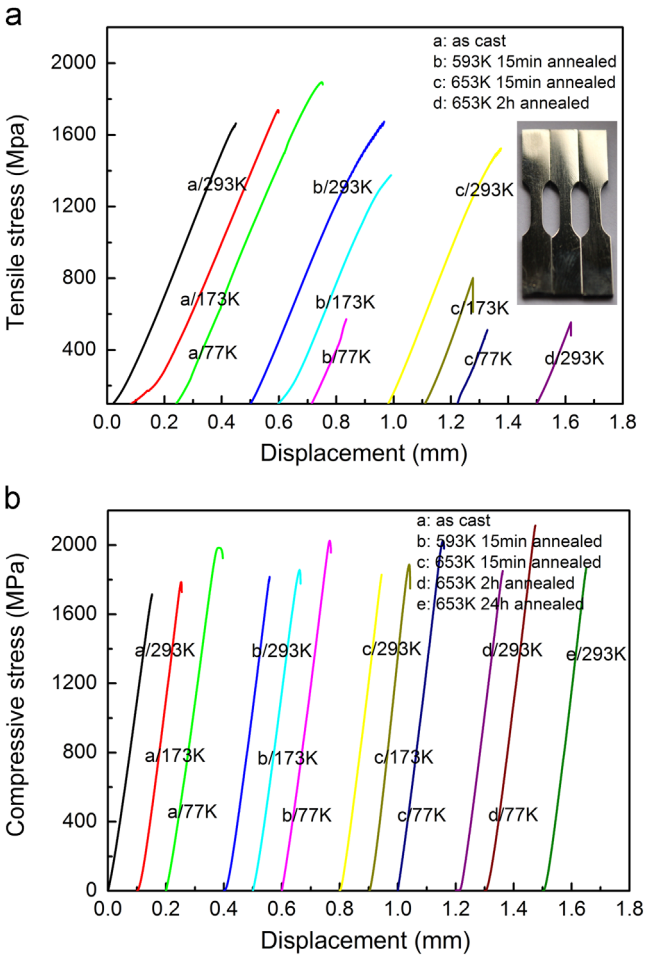

Fig. 1. The stress–displacement curves under (a) tension and (b) compression. The inset in (a) shows the real tensile samples.

The 1.5 mm thick plates were machined into the dog-bone geometry and the gauge dimensions of the samples were 6 mm in length, 1.2 mm in width and 1 mm in thickness. The 4 mm thick plates were machined into $3.5 \times 3.5 \times 7$ mm^3 samples for compressions. Some tensile and compression samples were sealed in evacuated quartz capsules and annealed below T_g (683 K at 20 K/min) to reduce the free volume concentration V_f, where V_f is the average free volume per particle and is dependent on the thermal historic state. Thus, there were five group samples labeled as "a", "b", "c", "d" and "e". Sample "a" was as-cast. Sample "b" was annealed at 593 K for 15 min. Samples "c", "d" and "e" were annealed at 653 K for 15 min, 2 h and 24 h, respectively. The X-ray diffraction (XRD) and high resolution transmission electron microscopy (HRTEM) results demonstrated that the present annealing treatments below T_g did not introduce crystallization. It should be noted that it was not easy to directly measure the value of V_f, while it is well known that prior to T_g, the exothermic event ΔH (i.e., the heat release during relaxation) is an indicator of the existence of free volume in BMGs [42]. There are$(\Delta H) = \beta' v_f$ with a constant β'. Differential scanning calorimeter (DSC) measurement can be done to obtain the ΔH of these five group samples. ΔV^* was defined as the required excess free volume to transition and should be at least larger than an atom volume. Then a reduced free volume $V_f/\Delta V^*$ can be obtained. Usually, a higher cooling rate will induce a larger V_f and larger $V_f/\Delta V^*$, whereas an annealing process will decrease them. The $V_f/\Delta V^*$ can be obtained to be 1/10 for the as-cast sample "a", 1/21 for sample "b", 1/25 for sample "c", ~1/30 for sample "d" and 1/30 for sample "e" based on the previous work [26] and the measured ΔH. Therefore, free volume $V_f/\Delta V^*$ in these samples decreases with increasing annealing temperature or time and decreases in order of samples "a", "b", "c", "d" and "e". Uniaxial tensile and compression tests were conducted using a computer-controlled SUNS CMT 5105 material testing machine with a nominal strain rate of 1×10^{-4} s^{-1} at RT and low temperatures (173 K and 77 K). The detailed test process is the same as that in Ref. [27]. The load and the crosshead displacement of the test machine were recorded. Usually, tension tests utilize dog-bone samples that are difficult to guarantee alignment, gripping, and edge effects. Similar problems can also be encountered in the compression tests. For the tensile tests, in order to mitigate the edge effect, four surfaces of the samples were carefully polished with fine SiC papers prior to the tensile testing. As for the alignment and gripping during the test, we have tried our best to ensure the accuracy and reliability of experimental data through testing more samples (at least six samples each). Similar dog-bone sample tests can also be found in other researchers' paper [18]. For the compression tests, a specimen jig was also used to carefully grind the two cut ends of the specimen, not only to ensure parallelism, but also to guarantee that the ends were as much as possible perpendicular to the longitudinal axis of the specimen, which is similar to the method described by Wu et al. [43]. Therefore, the experimental data should be acceptable when enough carefulness has been given by us during the sample preparation and testing. After tests, the fracture modes and fracture surface features of these tested samples were investigated with digital camera and scanning electron microscopy (SEM, JEOL Ltd JSM-6700F and HITACHI S-2700).

3. Results

3.1. Tensile tests

The engineering tensile stress–displacement curves of the samples are given in Fig. 1a. Here, the deviation of the slope might be due to the slide between the clamps and the sample. At RT (293 K), the

as-cast sample "a" shows a fracture strength σ_T^F (~1660 MPa) and its final fracture is along a single shear-band plane with a fracture angle θ_T of 53°, as shown in Fig. 2a. Clearly, it is a typical shear fracture mode [44]. The SEM observation demonstrates that the fracture surface of the sample "a" consists of a smooth region at the edge and a dominant region with micron-scale (~10 μm) cores and vein patterns (typical in Fig. 3a). It is accepted that the smooth region is caused by a sliding shear and the cores and vein patterns region is due to the subsequent catastrophic failure [45–47]. These results confirm the typical shear deformation and fracture feature of BMGs under tensions [44]. The sample "b" with less free volume V_f fails at a higher σ_T^F (~1704 MPa) and has the same shear mode (see Fig. 2b) and fracture surface feature as the sample "a". The sample "c" with further reduced V_f fails nearly in a normal tensile mode with the fracture plane approximately perpendicular to the stress axis (i.e., θ_T=87°), as shown in Fig. 2c. The σ_T^F is ~1521 MPa which is lower than those of samples "a" and "b". Moreover, its fracture surface displays a feature different from that of the shear fractured samples: the smooth region caused by the sliding shear disappears, and the fine dimples (~1.2 μm) become dominant patterns, as shown in

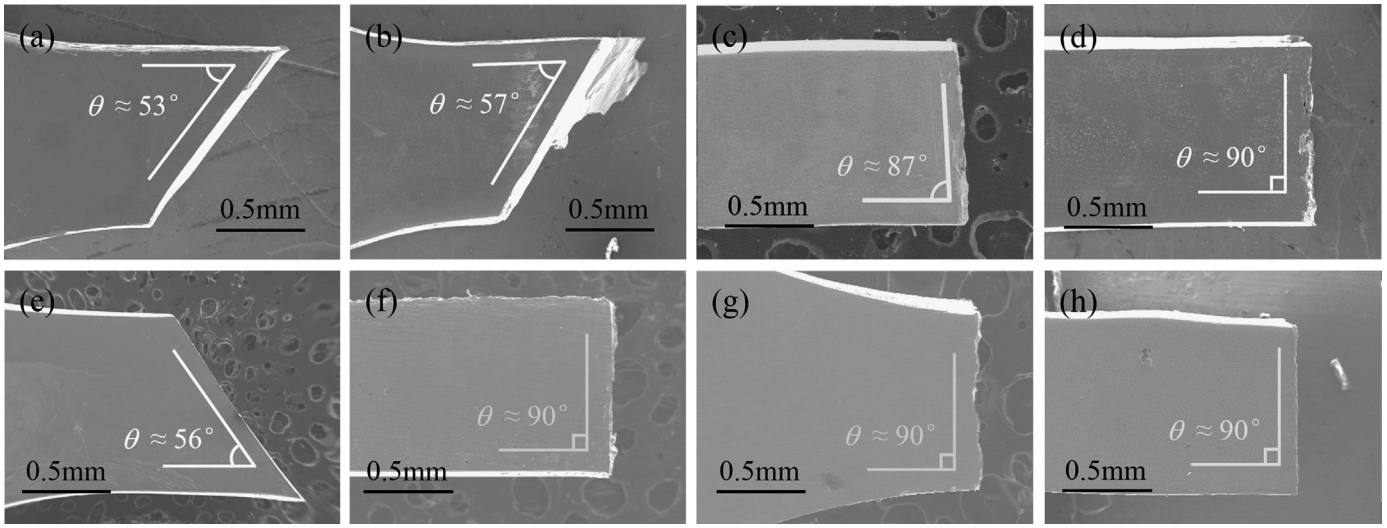

Fig. 2. Macroscopic fracture mode of samples under tension: (a–d) samples a, b, c and d at 293 K; (e–g) samples a, b and c at 77 K, and (h) sample c at 173 K.

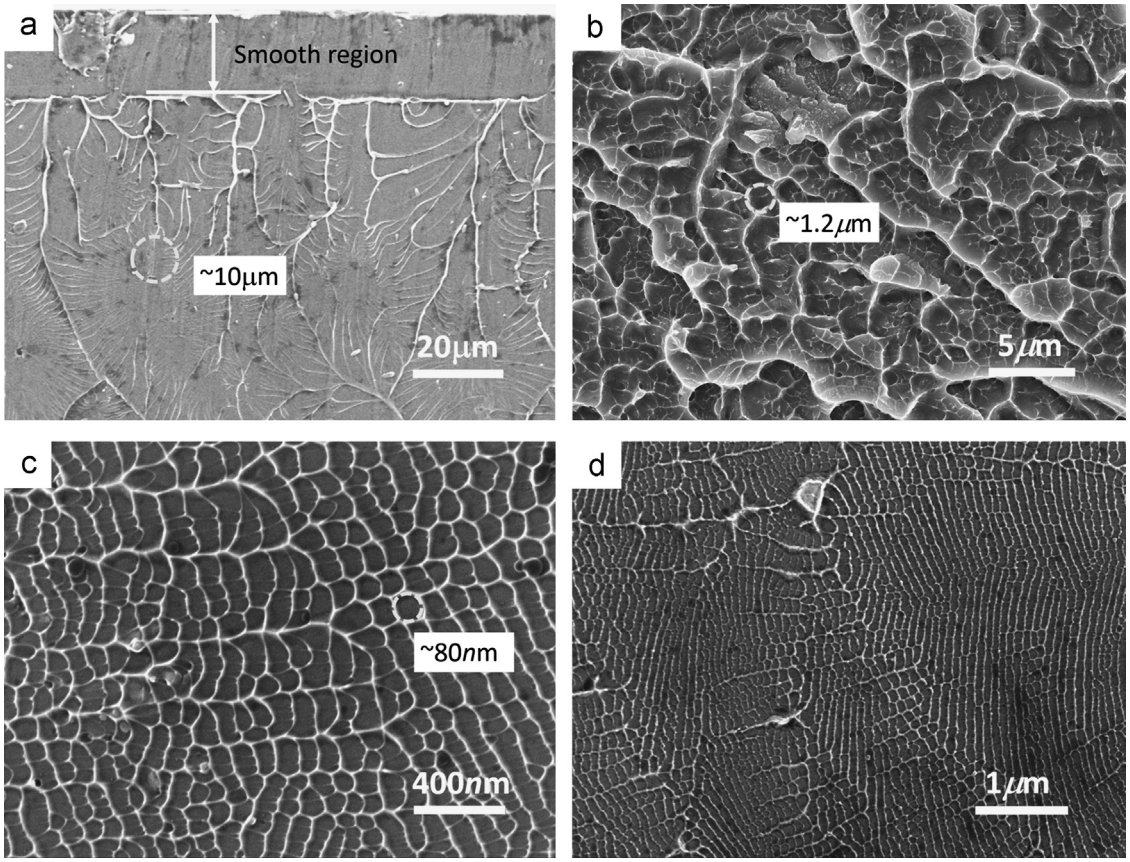

Fig. 3. Microscopic fracture surfaces of samples under tensions (a) smooth region and micron-scaled vein pattern in shear fracture surface, (b) fine dimple in normal tensile fracture surface, (c) nano-scale dimples and (d) nano-scale periodic corrugations in normal tensile fracture surface.

Fig. 3b. The sample "d" fails at a very low fracture stress σ_T^F (<600 MPa) in a normal tensile mode ($\theta_T=90^\circ$) as shown in Fig. 2d. Nano-scale dimples and even periodic corrugations ($\sim$80 nm) rather than micron-scale cores and vein patterns dominate on the fracture surface as shown in Fig. 3c and d, respectively. These nano-scale dimples and periodic corrugations are typical fracture features of quasi-brittle fracture of metallic glasses [25,48–50]. With further decreasing the temperature to 173 K and 77 K, the as-cast sample "a" fractures at higher σ_T^F ($\sim$1737 MPa and 1890 MPa) than that at RT but their fracture surface features remain micron-scale cores and vein patterns. For the sample "b" at 173 K, it shows a lower σ_T^F of 1388 MPa and fails approximately in a normal tensile mode. Even at 77 K, it fails at a very low fracture stress σ_T^F ($\sim$573 MPa) in a normal tensile mode, as shown in Fig. 2g. Fine dimples, nano-scale dimples and periodic corrugations are the dominant patterns on the fracture surface of sample "b" at 173 K and 77 K, respectively. The sample "c" fails in a normal tensile mode at both 177 K and 77 K, and σ_T^F were $\sim$801 MPa and $\sim$512 MPa, respectively. Their fracture surface features are also nano-scale dimples and periodic corrugations. It should be noted that the sample "e" at all temperatures and sample "d" at low temperatures were too brittle to withstand tensile tests. The measured σ_T^F values in a shear fracture mode were stable, while more scattered in a normal tensile mode. A similar phenomenon has also been observed in the as-cast Vit1 BMG under tensions at room temperature (300 K) down to liquid helium temperature (4.2 K) [37].

3.2. Compression tests

The engineering stress–displacement curves of the compressive samples are presented in Fig. 1b. At RT, all the samples show no obvious macroscopic plastic deformation. And their fracture stresses σ_C^F increase with decreasing V_f (increasing annealing temperature or prolonging annealing time). The as-cast sample "a" fails in a shear mode with the fracture angles θ_C of about 43°, as shown in Fig. 4a. The samples "b" and "c" also fail in the same shear mode as that of sample "a". With further decreasing V_f (prolonging annealing time), the samples fail through breaking into three pieces (see sample "d") and even a lot of fine fragments (see sample "e"), as shown in Fig. 4b and c, respectively. This fragmentation mode has also been found in other brittle BMGs (Mg-, Fe- and Co-based) under compressions [48,50–52]. At low

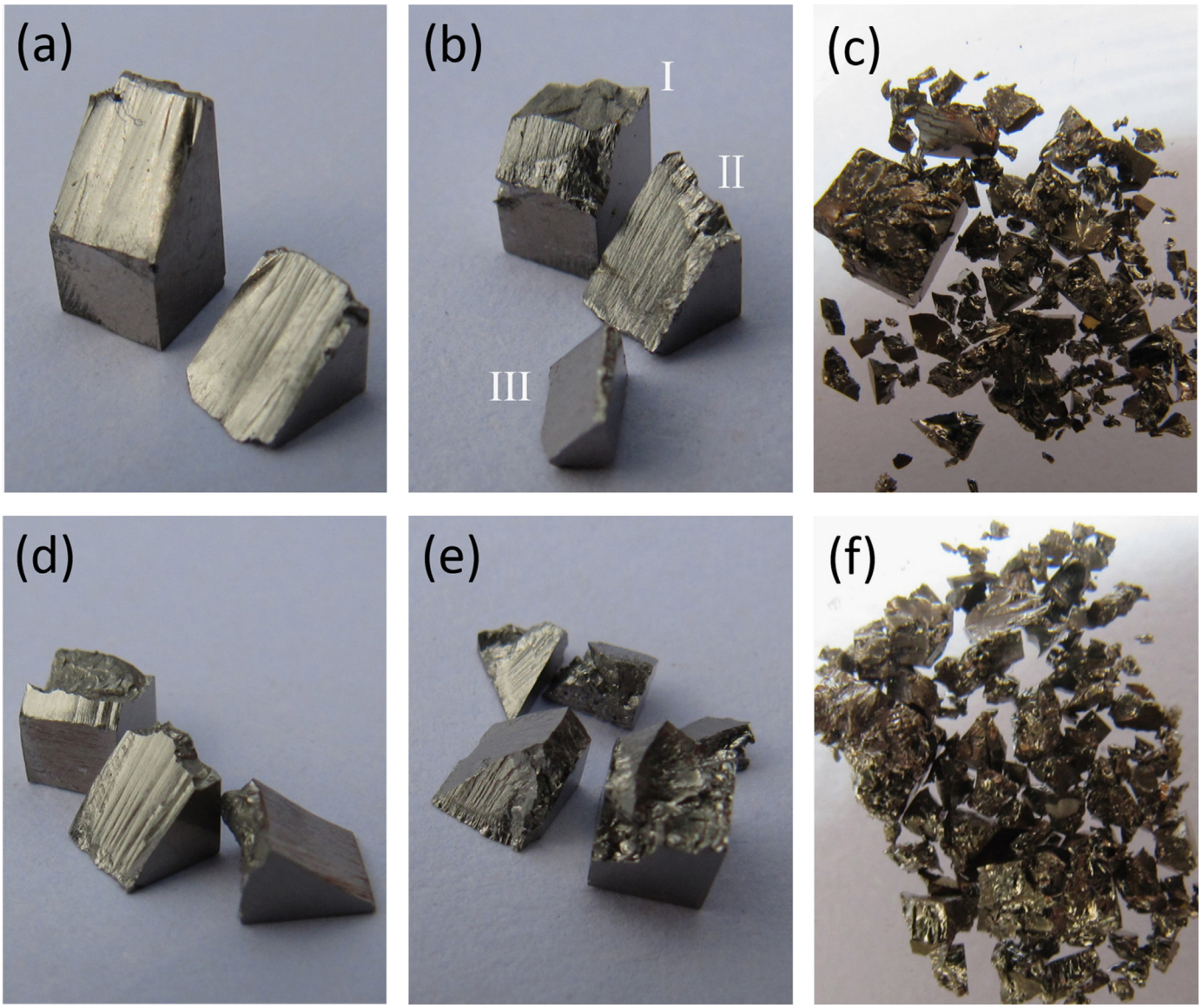

Fig. 4. Macroscopic fracture mode of samples under compression: (a) sample "a" at 293 K shear fractured into two parts, (b) sample "d" at 293 K first shear and then normal tensile fractured into three pieces, (c) sample "e" at 293 K fractured into many pieces, (d–f) samples "b","c" and "d" at 77 K broke into three pieces even many pieces.

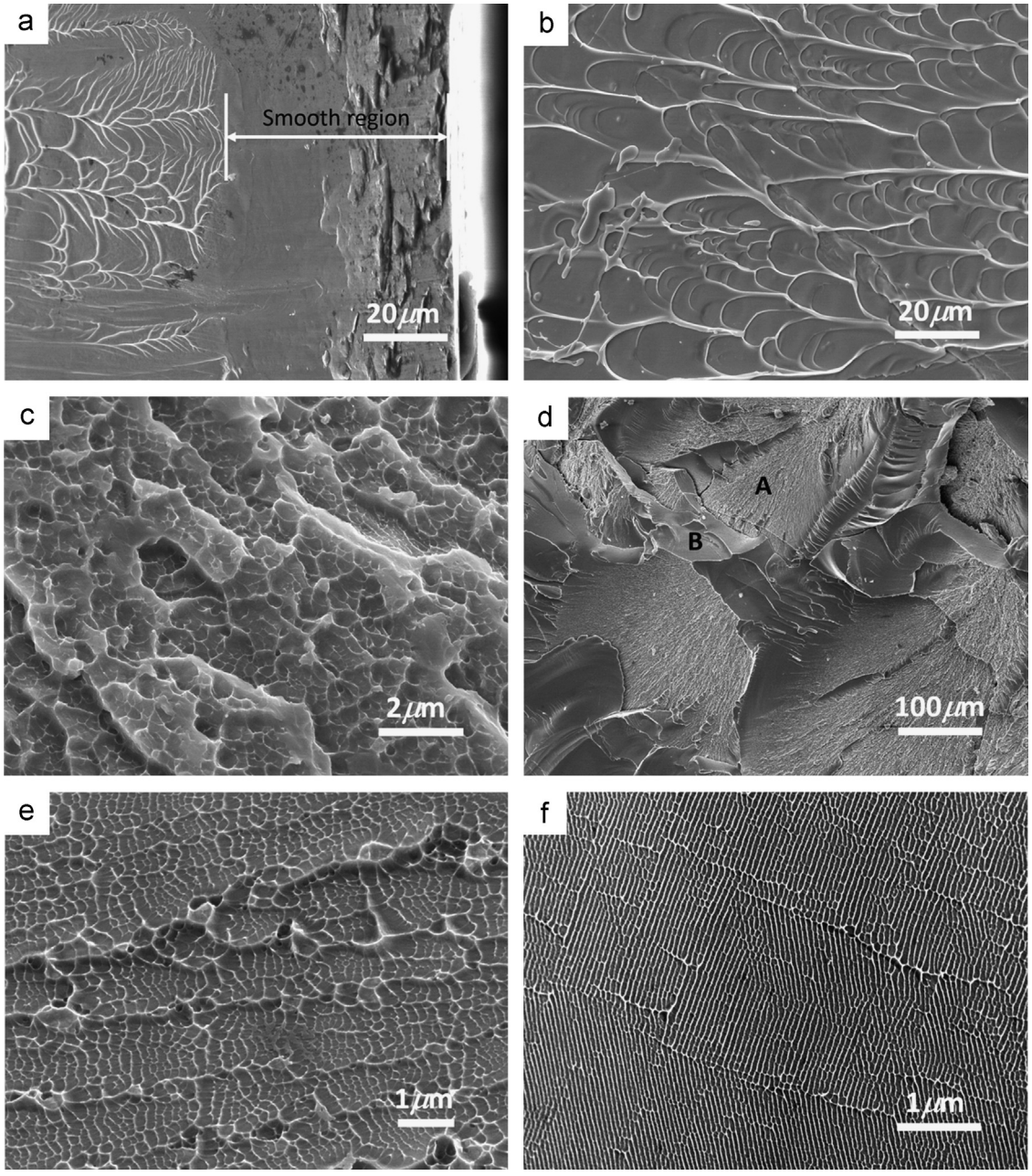

Fig. 5. (a) The fracture surface of the sample failed in shear mode containing a smooth region and micron-scale vein patterns. (b) The shear feature in the surface of samples in mixed fracture mode. (c) The tensile fracture feature in the surface of samples in mixed fracture mode. (d) The fine dimple feature in the tensile fracture surface marked "A". (e) The nano-scale dimple feature in the tensile fracture surface marked "B". (f) Nano-scale periodic corrugations in the tensile fracture surface.

temperatures (173 K and 77 K), the as-cast sample "a" shows a higher σ_C^F, but also displays an obvious yield behavior with enhanced plasticity than that at RT and finally fails in a shear mode. These results are consistent with other reported results at lower temperatures (down to liquid nitrogen temperature 77 K) [11–14,16]. However, for the samples "b" and "c" with reduced free volume concentration, their σ_C^F increase but the fracture modes change from shear (sample "b" at 293 K and 173 K, sample "c" at 293 K) to breaking into three pieces (sample "b" at 77 K, sample "c" at 173 K) and even a lot of small fragments (sample "c" at 77 K), with decreasing temperature (as shown in Fig. 4d–f). For the present samples with shear fracture into two parts as illustrated in Fig. 5a, a smooth region exists at the fracture surface edge and micron-scale vein pattern regions dominate in the two fracture surfaces, which is in agreement with those of other tough BMGs [44,46,53]. This smooth region is also caused by the shear sliding and the micron-scale vein pattern results from the subsequent catastrophic failure under compressions. For the samples failed into three pieces as shown in Fig. 4b, the three parts are termed as parts I, II and III. Part I has a shear fracture surface with micron-scale vein patterns as shown in Fig. 5b. Part II has two different fracture surface features: the surface matched with part I has the same shear fracture features and the other fracture surface (Fig. 5c) matched with Part III shows fine dimples (marked as A) as shown in Fig. 5d and nano-scale dimples (marked as B) as shown in Fig. 5e. For the samples broken into many fine fragments, small area fraction of shear feature and large area fraction of tensile feature (nano-scale dimples and periodic corrugations in Fig. 5f) are found in the fracture surfaces. During the uniaxial compressive loading, the tensile stress will gradually increase from zero due to the shear induced dilatation [5,54]. The samples under uniaxial compressions should first shear, and then continue to fail

in shear fracture mode or tensile fracture mode, which mode to occur depends on the competition between shear stress and it-induced tensile stress. If tensile stress becomes dominant, the sample will break into three or more parts. Therefore, nano-scale dimples can be seen on the fracture surface of some parts, At the same time, micron-scale vein patterns can be found on other firstly sheared fracture surface. If the shear stress always dominates the fracture, only vein patterns can be observed on the entire fracture surface. In fact, such a mechanism is essentially consistent with that in the uniaxial tension case, where the intrinsic competition between shear and it-induced tension/dilatation is also at work [37]. This has been verified by the macroscopic fracture patterns and the microscopic fracture feature as shown in Figs. 4 and 5, respectively.

3.3. Fracture toughness

Here, fracture toughness is not directly measured but just estimated from fracture surface features. It has been widely accepted that the ridge spacing (w) found on the fracture surface can be used to estimate the fracture toughness (K_c) by the Dugdale approximation [38,48,55]:

$$K_c = \sigma_y \sqrt{6\pi w} \quad (1)$$

where σ_y is the tensile yield strength and could be approximately equal to σ_T^F for the present samples due to no significant strain hardening. Fig. 6a shows the values of the measured fracture strength (σ_T^F) and the calculated fracture toughness (K_c) of samples "a", "b", "c" and "d" at RT. It could be seen that, compared with the as-cast sample "a", σ_T^F and K_c of sample "b" with less free volume increase slightly.

Here, the estimated fracture toughness is closely related to strength and ridge spacing (w). Since the ridge spacings of sample "b" and sample "a" (as-cast) are similar, and the strength of sample "b" is large sample "a" due to less free volume, the estimated fracture toughness of sample "b" will be larger than that of sample "a". Decreasing free volume further, σ_T^F and K_c dramatically decrease (see samples "c" and "d"), with the transition of the macroscopic fracture modes from ductile shear fracture to brittle normal tensile fracture and the length scale of microscopic fracture feature from micron to nanometer also take place. It is clear that there is a DBT due to the decrease of the free volume. Fig. 6b presents the values of σ_T^F and K_c of samples "a", "b" and "c" at different temperatures. For the as-cast sample "a", with the decrease of temperature, its σ_T^F and K_c slightly increase, which is in agreement with recent reports [37]. Accordingly, its fracture mode and fracture surface features do not change, indicating that no DBT behavior occurs in the present temperature range. However, for the sample "b", with the decrease of temperature, the values of σ_T^F and K_c dramatically reduce, and the fracture mode and the fracture surface features change correspondingly. Its DBTT is between 177 K and 77 K. Similarly, there is DBT behavior for sample "c" with decreasing temperature and its DBTT is between 177 K and

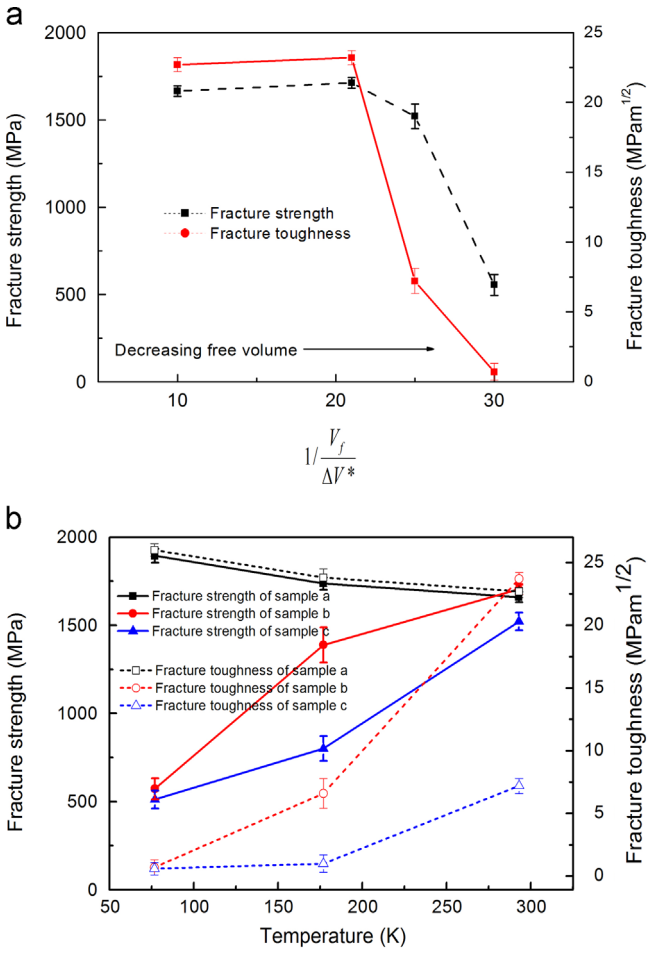

Fig. 6. Tensile fracture strength and fracture toughness of (a) samples with different free volume states at room temperature (b) samples a, b and c at different temperatures.

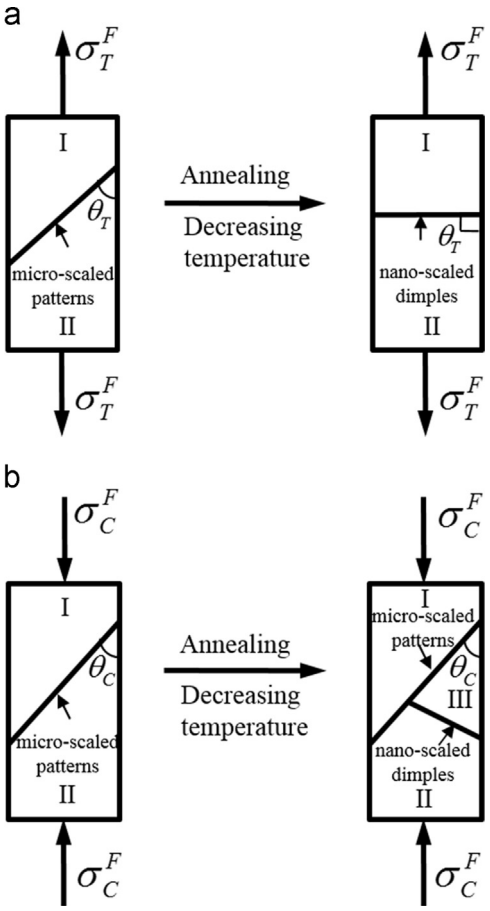

Fig. 7. The schematic illustration of the alteration of fracture mode and fracture surface features due to annealing and decreasing temperature under (a) tension and (b) compression.

Table 1
Mechanical properties and parameters of the Vit105 BMG.

Samples/test temperature	Compression		Tension		Parameters				K_c/MPa$\sqrt{m}$
	σ_C^F (MPa)	θ_C	σ_T^F (MPa)	θ_T	τ_0 (MPa)	σ_0 (MPa)	α	σ_C^F/σ_T^F	
a/RT	1726	43°	1660	53°	863	3220	0.27	1.04	22.7
b/RT	1817	43°	1704	56°	909	2606	0.33	1.06	23.7
c/RT	1824	43°	1521	87°	912	1521	0.60	1.20	7.2
d/RT	1863	Shear+tensile	555	90°	930	555	1.67	3.36	0.7
e/RT	1876	Split	–	–	939	–	–	–	
a/173 K	1786	43°	1737	56°	893	3720	0.24	1.03	23.8
b/173 K	1851	43°	1388	90°	926	1388	0.67	1.33	6.6
c/173 K	1882	43°	801	90°	941	801	1.17	2.35	1.0
a/77 K	1980	43°	1894	56°	990	3414	0.29	1.045	26.0
b/77 K	2030	Shear+tensile	573	90°	1015	573	1.77	3.54	0.7
c/77 K	2028	Split	512	90°	1014	512	1.98	3.96	0.6

RT. Certainly, more tests at different temperatures are useful to more precisely determine the DBTT of these samples. Nevertheless, the present results apparently show that the DBTT could increase with decreasing free volume concentrations.

4. Discussion

According to the above experimental observations, we could see that either annealing, i.e., decreasing free volume V_f or decreasing test temperature could induce the DBT behavior, which is confirmed by the transition of the macroscopic fracture modes from ductile shear to brittle normal tension (as schematically illustrated in Fig. 7a) and the length scale of microscopic fracture morphologies from micron to nanometer under tensions. Similarly, under compression, ductile shear fracture mode can change into brittle split mode. And the micron-scale vein patterns will transfer into nano-scale dimples and even nano-scale periodic corrugations. It is obvious that there are two kinds of competitions: macroscopic fracture mode between the shear fracture (mode II) and the normal tensile fracture (mode I), and microscopic fracture feature between micron-scale vein patterns and nano-scale dimples or periodic corrugations. Here, the fracture angles are shown to be changing from 53 degrees to 90 degrees from the as-cast to the annealed condition. However, an abrupt change from 57 to 87 degrees does not constitute a transition. In fact, such a transition point from shear to tension has been experimentally verified in another Zr-based BMG (Vit1) by our recent work [37], where fracture angles changed from 56, 59, 60, 61, 72, to 87 (almost 90) degrees due to the test temperature decreasing from room temperature (300 K) down to liquid helium temperature (4.2 K). More tests indicating the transition will be carried out in the future work.

Additionally, it should be noted that the validation of Dugdale approximation to estimate the fracture toughness through the fracture surface features might be questionable when different fracture mechanisms have been involved in these samples. In general, ductility is a solid material's ability to deform under tensile stress. Here, the monolithic BMGs present zero tensile plastic deformation. This means BMGs are inherently brittle rather than ductile. Some BMGs exhibit good fracture toughness while some exhibit poor fracture toughness. The former is called ductile BMG and the latter is the brittle one, which has been mentioned by Ramamurty group in their recent papers [56–58]. Here, DBT of BMGs was defined as the transition of microscopic fracture feature and macroscopic fracture mode. This definition is more intrinsic than that based on the macroscopic plastic strain or measured fracture toughness or compact toughness. The present estimation of fracture toughness is subordinate to help in better understanding the DBT behavior. In fact, without the estimation of fracture toughness, the DBT behavior of BMGs can still be determined based on the above transitions.

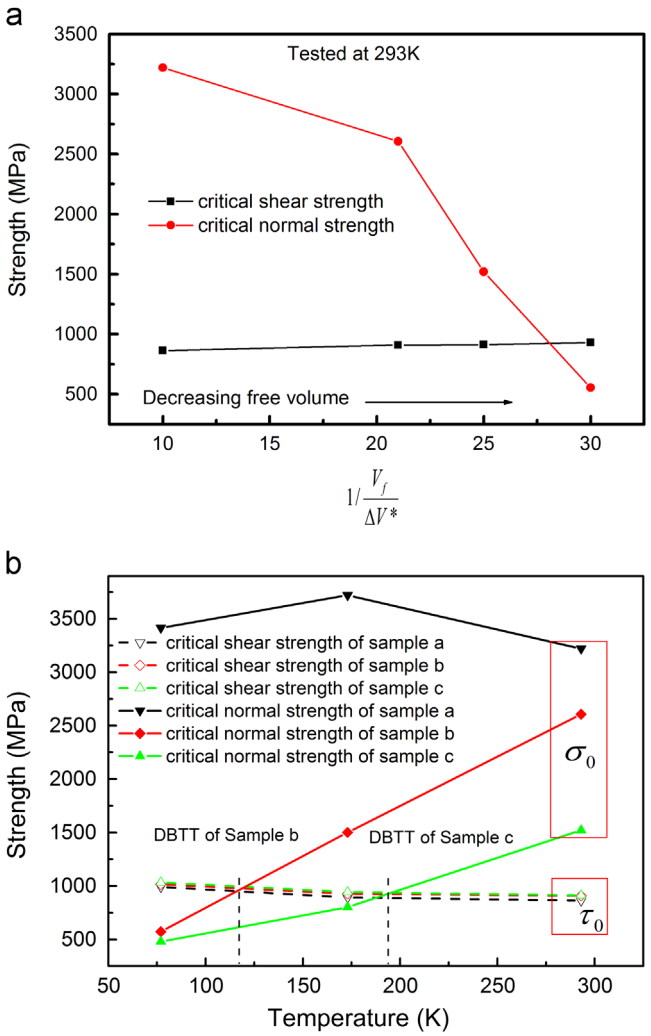

Fig. 8. The critical shear and normal strength of (a) samples with different free volumes at RT (b) samples at different temperatures.

4.1. Macroscopic fracture mode transition

It is well known that the occurrence of either shear fracture or normal tensile fracture depends on which process requires the smaller applied stress, i.e., the shear stress and the normal stress.

τ_0 and σ_0 have been defined as the intrinsic critical strengths of a material in a mode II fracture (shear fracture) and in a mode I failure (normal tensile fracture), respectively [27,59]. Following the unified fracture criterion [59], τ_0 and σ_0 could be calculated based on the measured experimental values of σ_T^F, σ_C^F, θ_T and θ_C, which are listed in Table 1.

Fig. 8a presents the variation of τ_0 and σ_0 with the free volume V_f. It is found that τ_0 decreases and σ_0 increases with decreasing free volume. At a critical free volume V_f^c, the transition of fracture mode, i.e., shear fracture to normal tensile fracture could be anticipated. In Fig. 8b, for the sample "b", the critical shear strength τ_0 will slightly increase from 909 MPa to about 1015 MPa and normal tensile strength σ_0 dramatically decreases from ~2606 MPa to ~573 MPa with the decrease of the test temperature from 293 K to 77 K, indicating that the shear fracture (mode II failure) occurs with more difficultly and the tensile fracture (mode I failure) becomes easier to occur. At a critical temperature (about 118 K), the macroscopic mode of failure might change from ductile shear fracture (model II) to brittle tensile fracture (mode I failure). Similarly, for the sample "c", the DBTT could be determined to be about 194 K, while for the sample "a", the critical shear strength τ_0 is always lower than the critical normal strength σ_0, indicating that no DBT would take place in the test temperature range. It could be expected that its DBTT should be much less than 77 K. It is obvious that either annealing (decreasing free volume) or decreasing temperature will enhance the critical shear strength τ_0, but reduce the critical normal strength σ_0, which results in the DBT of BMGs.

4.2. Microscopic fracture feature transition

The experimental results clearly show that two different facture mechanisms exist in BMGs, which are indicated by micron-scale vein patterns on the fracture surface as ductile fracture and nano-scale dimples/periodic corrugations on fracture surfaces as brittle fracture. It is well known that tough metallic glasses fail by shear banding and brittle metallic glasses rupture due to cracking. The shear band is generally deflected to the original crack plane and the deflection angle is usually more than 45° under tensile loading, while the brittle crack path is almost perpendicular to the normal stress [27]. In order to further understand the two fracture modes in BMGs, Fig. 9 schematically illustrates the underlying mechanism on the basis of the experimental observations. For the as-cast sample "a" a number of free volume would aid STZs to activate and evolute, leading to the shear band formation. Where the shear band begins to slide stably under a shear stress, core nucleation and growth occurs within the shear band due to the normal stress component of loading. The shear band grows unstably and breaks rapidly when the core reaches a critical value. Thus, a smooth region, round cores and vein-like patterns with radiating ridges appear on the fracture surface (Fig. 3a). For brittle fracture (e.g., samples "c" and "d" or sample "b" tested at cryogenic temperature), atomic cluster motions become very difficult due to stronger stiffness of the atomic bond, so the shear band creation should be suppressed. Brittle crack propagation controls the brittle facture by an intrinsic cavitation mechanism in the vicinity of the crack tip [60–61]. Cavitation is associated with propagation of a self-sharpening crack tip, because multiple voids nucleated continuously under normal stress, leaving nanometer dimples/periodic corrugations on the fracture surface (Fig. 3(b-d) Fig. 5(c-f).

4.3. The DBT map of BMG

The DBT behavior of crystalline alloys (e.g., body centered cubic metals and alloys) is usually due to the competition between the

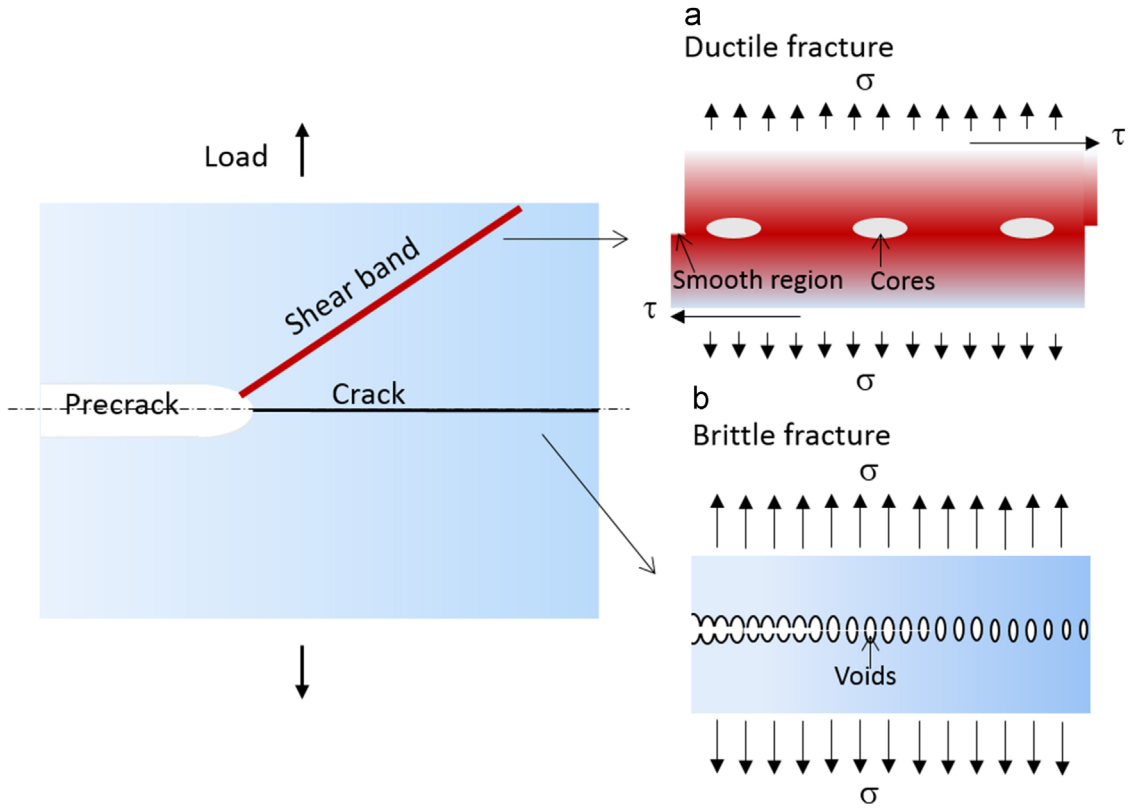

Fig. 9. Schematic illustration of fracture mechanism in BMGs. (a) The shear band sliding experiences both normal and shear stress component of loading in ductile fracture and (b) the crack propagation under normal stress in brittle fracture.

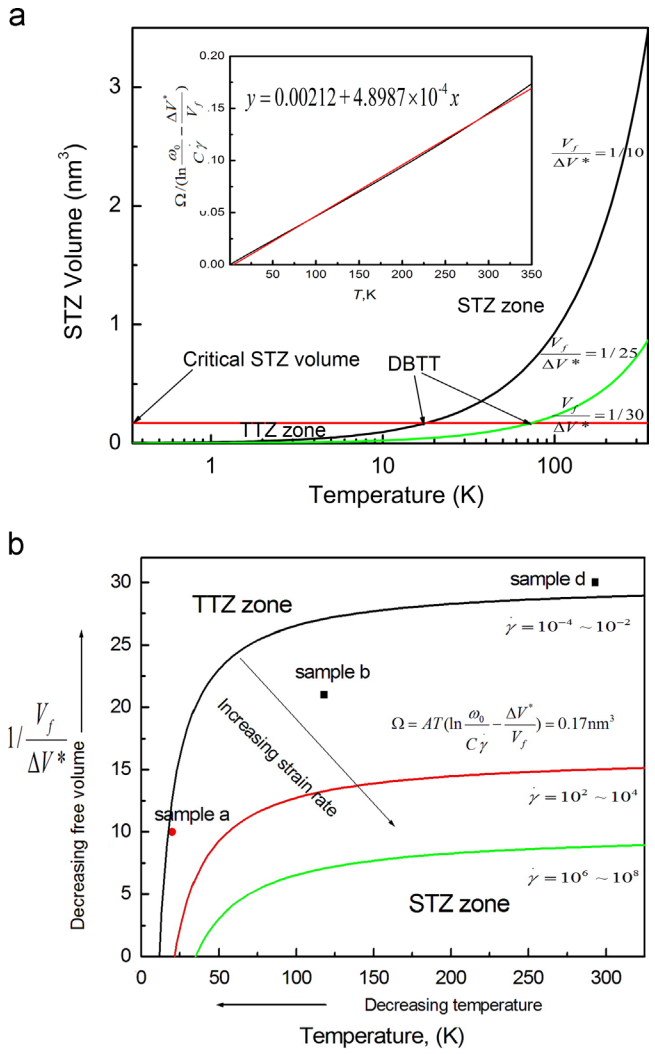

Fig. 10. (a) Variation of STZ volume with temperature T for different free volume states. (b) The DBT map of BMGs. The inset of (a) shows variation of $\Omega/(\ln(\omega_0/C\dot\gamma)-(\Delta V^*/V_f))$ with temperature T.

dislocation emission (flow) and cleavage (crack propagation). However, the DBT of BMGs might be attributed to the competition between STZs and tension transformation zones (TTZs) [49]. The STZ operation actually is a local motion of atoms (clusters) around a free volume site as the unit process of plastic flow, while the TTZ is essentially a local atomic cluster with smaller relaxation time-scales and less visco-plasticity, and the TTZ operation corresponds to the volume dilatation through the rupturing of cluster to form nano-scale voids [49]. Through TTZs, stored energy is dissipated mainly by the new surface formation, resulting in the brittle fracture of metallic glasses. Conversely, STZ-mediated deformation always leads to the ductile fracture of metallic glasses where significant plastic flow occurs ahead of the crack tip [20,62–63]. Therefore, the ductile-to-brittle transition (DBT) of metallic glasses can be well understood within the picture of STZ versus TTZ of atomic cluster motions [25,27,49,64].

Our recent paper has shown that the DBT under three-point bending could be achieved through either annealing sample or decreasing test temperature for the Zr-based BMG. And the STZ volume (Ω) as an indicator was proposed to quantitatively characterize the DBT behavior in fracture of metallic glasses [26]. When the STZ volume Ω is extremely small or close to zero, it would need a large number of STZ and might be hard to synchronously cooperate shear to generate a shear band, therefore brittle TTZ mode would occur instead of the STZ mode. In this sense, the STZ volume Ω could be a key to generate shear bands and thus shear deformation.

For a specific BMG, the STZ volume Ω can be expressed by [26]

$$\Omega = \frac{k}{4R\zeta\mu_T\gamma_T^2(1-2\mu_T\gamma_T/(\pi\mu_0\gamma_0))^{3/2}}T\left(\ln\frac{\omega_0}{C\dot\gamma}-\frac{\Delta V^*}{V_f}\right) \quad (2)$$

where constant R is the "fold ratio" $\approx 1/4$ and $\zeta=3$ is a correction factor, ω_0 is an attempt frequency, C is a dimensionless constant of order unity, k is the Boltzmann constant and T is the temperature. μ_0 is the athermal shear modulus and $\gamma_0=0.036$. μ_T is the temperature-dependent shear modulus $\gamma_T=0.036-0.016(T/T_g)^{2/3}$. The detailed definition or value of R, ζ, μ_T, γ_T, μ_0, γ_0, C, ω_0, k, $\dot\gamma$ can be found in Refs. [26,40]. Eq. (2) indicates that Ω is mainly dependent on three factors: test temperature T, strain rate ($\ln(\omega_0/C\dot\gamma)$) and free volume ($V_f/\Delta V^*$). In the quasi-static strain rate range ($\dot\gamma\approx10^{-4}\sim10^{-2}$ s^{-1}), $\ln(\omega_0/C\dot\gamma)=30$ [40]. There is $1/30\le V_f/\Delta V^*\le 1/10$, corresponding to different free volume states between the glassy sample which is very close to its crystalline counterpart from the viewpoint of energy landscape [65,66] and the as-cast sample. In particular, with decreasing V_f, $V_f/\Delta V^*$ decreases and would be approaching 1/30.

For the different free volume contents $V_f/\Delta V^*$, the variation of Ω with T could be plotted as shown in Fig. 10a. It is found that Ω decreases with the decreasing temperature T. It had been suggested that when Ω decreases to a very small value such as a critical $\Omega=0.17$ nm^3 which involves several atoms, STZ might not form and TTZ is activated instead [26], we have

$$f(T) = \frac{k}{4R\xi\mu_T\gamma_T^2(1-2\mu_T\gamma_T/(\pi\mu_0\gamma_0))^{3/2}}T \quad (3)$$

Then Eq. (2) can be

$$\Omega/\left(\ln\frac{\omega_0}{C\dot\gamma}-\frac{\Delta V^*}{V_f}\right) = f(T) \quad (4)$$

For the present Vit105 BMG, the variation of $\Omega/(\ln(\omega_0/C\dot\gamma)-(\Delta V^*/V_f))$ with T is shown in the inset of Fig. 10a. For simplicity, the curve could be linearly fitted to be $y=0.00212+4.8987\times10^{-4}x$. Thus Eq. (4) becomes

$$\Omega = AT\left(\ln\frac{\omega_0}{C\dot\gamma}-\frac{\Delta V^*}{V_f}\right) \quad (5)$$

here $A=4.8987\times10^{-4}$ nm^3/K. It is expected $\Omega=0.17$ nm^3 of the critical STZ volume for TTZ activation. Then we have

$$DBTT = 347\text{ K}/\left(\ln\frac{\omega_0}{C\dot\gamma}-\frac{\Delta V^*}{V_f}\right) \quad (6)$$

The relationship between DBTT and free volume term ($V_f/\Delta V^*$) in the quasi-static strain rate range could be given in Fig. 10b (the dark curve). The upper part of the solid curve is corresponding to the brittle zone (TTZ zone), and the lower part to the ductile zone (STZ zone). It is clear that with decreasing temperature, the ductile zone will approach the brittle zone, indicating the DBT. At the same time, decreasing free volume by annealing, the brittle zone can be easily reached at higher temperatures. For example, as to the as-cast sample with larger number of free volume ($V_f/\Delta V^*=1/10$), it is predicted that extremely low temperature of about 17 K was needed to introduce DBT. This theoretical prediction is in agreement with our recent observations, where a DBT has been identified in an as-cast Vit1 BMG under tensions at about 20 K [37]. For the annealed sample "b" with less free volume, its DBTT increases to about 118 K according to the experimental results, as shown in Fig. 8b. Even for the well annealed sample "d", DBT will occur at RT. Again, the DBTT can be enhanced by annealing samples and is closely related with the free volume state in the samples. Of course, there is discrepancy between the predicted DBTT and measured values, more test at

different temperatures and accurate measurement of free volume concentration are desirable.

Additionally, it has been reported that the tough BMGs would be embrittled and even suffered a DBT as loading at high strain rates [49,64,66]. We can obtain the red curve (for $\dot{\gamma} \approx 10^2$–$10^4$ s^{-1}) and green curve (for $\dot{\gamma} \approx 10^6$–$10^8$ s^{-1}) based on Eq. (6). It indicates that the brittle zone would increase with increasing strain rate. For a sample with a fixed initial free volume, the DBTT can also be increased by increasing the strain rate. Obviously, if decreasing free volume and increasing strain rate are simultaneously adopted, the DBT will take place more readily. On the contrary, brittle BMGs might exhibit ductility when the ambient temperature is higher than their DBTT or their free volume concentration can be restored such as by recovery quench [28,67].

5. Conclusion

Uniaxial tensile and compression tests for the Zr-based (Vit105) BMG with different free-volume states were performed at RT and cryogenic temperatures. We confirm a significant DBT behavior, which is accompanied by the change of macroscopic fracture modes from ductile shear fracture to brittle normal tensile fracture and microscopic fracture features from micron-scale vein patterns to nano-scale dimples and even periodic corrugations. Either annealing (decreasing free volume) or decreasing temperature will enhance the critical shear strength τ_0 and reduce the critical normal strength σ_0, leading to the DBT of BMGs. A DBT map for BMGs is proposed based on the STZ volume as an indicator, taking into account three factors (ambient temperature, free volume and strain rate). After this, many previous works which have investigated individually the single effect of temperature, free volume (annealing or cooling rate) and strain rate on the DBT of metallic glass can be united for consideration under this frame. This is useful to understand the deformation and fracture mechanism of BMGs and will provide a strategy to tune the mechanical properties and guide the application of bulk metallic glasses.

Acknowledgment

The financial support from the National Natural Science Foundation of China (NSFC) under Grant nos. 51171138, 11372315 and 51321003 are gratefully acknowledged. The work was supported by Ph.D. Programs Foundation of Ministry of Education of China (20110201110002).

References

[1] W.L. Johnson, MRS Bull. 24 (1999) 42.
[2] A. Inoue, Acta Mater. 48 (2000) 279.
[3] C.A. Schuh, T.C. Hufnagel, U. Ramamurty, Acta Mater. 55 (2007) 4067.
[4] C.J. Gilbert, R.O. Ritchie, W.L. Johnson, Appl. Phys. Lett. 71 (1997) 476.
[5] J.H. Schneibel, J.A. Horton, P.R. Munroe, Metall. Mater. Trans. A 32 (2001) 2819.
[6] J. Schroers, W.L. Johnson, Phys. Rev. Lett. 93 (2004) 255506.
[7] P. Wesseling, T.G. Nieh, W.H. Wang, J.J. Lewandowski, Scr. Mater. 51 (2004) 151.
[8] X.J. Gu, S.J. Poon, G.J. Shiflet, J.J. Lewandowski, Acta Mater. 58 (2010) 1708.
[9] Q. He, Y.Q. Cheng, E. Ma, J. Xu, Acta Mater. 59 (2011) 202.
[10] M.D. Demetriou, M.E. Launey, G. Garrett, J.P. Schramm, D.C. Hofmann, W. L. Johnson, R.O. Ritchie, Nat. Mater. 10 (2011) 123.
[11] H.Q. Li, K.X. Tao, C. Fan, P.K. Liaw, H. Choo, Appl. Phys. Lett. 89 (2006) 041921.
[12] A. Kawashima, T. Okuno, H. Kurishita, W. Zhang, H. Kimura, A. Inoue, Mater. Trans. 48 (2007) 2787.
[13] Y.J. Huang, J. Shen, J. Sun, Z.F. Zhang, Mater. Sci. Eng. A 498 (2008) 203.
[14] T. Okuno, A. Kawashima, H. Kurishita, W. Zhang, H. Kimura, A. Inoue, Mater. Trans. 49 (2008) 513.
[15] A. Vinogradov, A. Lazarev, D.V. Louzguine-Luzgin, Y. Yokoyama, S. Li, A. R. Yavari, A. Inoue, Acta Mater. 58 (2010) 6736.
[16] K.S. Yoon, M. Lee, E. Fleury, J.C. Lee, Acta Mater. 58 (2010) 5295.
[17] A. Kawashima, Y. Yokoyama, I. Seki, H. Kurishita, M. Fukuhara, H. Kimura, A. Inoue, Mater. Trans. 50 (2009) 2685.
[18] L.S. Huo, H.Y. Bai, X.K. Xi, D.W. Ding, D.Q. Zhao, W.H. Wang, R.J. Huang, L.F. Li, J. Non-Cryst. Solids 357 (2011) 3088.
[19] J. Yi, S.M. Seifi, W. Wang, J.J. Lewandowski, J. Mater. Sci. Technol. 30 (2014) 627.
[20] C.A. Pampillo, D.E. Polk, Acta Metall. 22 (1974) 741.
[21] A.R. Yavari, Mater. Sci. Eng. 98 (1988) 491.
[22] T.W. Wu, F. Spaepen, Philos. Mag. B 61 (1990) 739.
[23] E.P. Barth, F. Spaepen, R. Bye, S.K. Das, Acta Mater. 45 (1997) 423.
[24] R. Raghavan, P. Murali, U. Ramamurty, Intermetallics 14 (2006) 1051.
[25] R. Raghavan, P. Murali, U. Ramamurty, Acta Mater. 57 (2009) 3332.
[26] F. Jiang, M.Q. Jiang, H.F. Wang, Y.L. Zhao, L. He, J. Sun, Acta Mater. 59 (2011) 2057.
[27] G. Li, M.Q. Jiang, F. Jiang, L. He, J. Sun, Appl. Phys. Lett. 102 (2013) 171901.
[28] G. Kumar, D. Rector, R. Conner, J. Schroers, Acta Mater. 57 (2009) 3572.
[29] D.I. Uhlenhaut, F.H. Dalla Torre, A. Castellero, C.A.P. Gomez, N. Djourelov, G. Krauss, B. Schmitt, B. Patterson, J.F. Loeffler, Philos. Mag. 89 (2009) 233.
[30] X. Gu, S. Poon, G. Shiflet, J. Lewandowski, Scr. Mater. 60 (2009) 1027.
[31] F. Jiang, H.F. Wang, M.Q. Jiang, G. Li, Y.L. Zhao, L. He, J. Sun, Mater. Sci. Eng. A 549 (2012) 14.
[32] A.L. Greer, Y.Q. Cheng, E. Ma, Mater. Sci. Eng. R 74 (2013) 71.
[33] J.J. Lewandowski, W.H. Wang, A.L. Greer, Philos. Mag. Lett. 85 (2005) 77.
[34] J.J. Lewandowski, M. Shazly, A.S. Nouri, Scr. Mater. 54 (2006) 337.
[35] A. Castellero, B. Moser, D.I. Uhlenhaut, F.H. Dalla Torre, J.F. Loeffler, Acta Mater. 56 (2008) 3777.
[36] G. Kumar, D. Rector, R.D. Conner, J. Schroers, Acta Mater. 57 (2009) 3572.
[37] M.Q. Jiang, G. Wilde, J.H. Chen, C.B. Qu, S.Y. Fu, F. Jiang, L.H. Dai, Acta Mater. 77 (2014) 248.
[38] S.V. Madge, D.V. Louzguine-Luzgin, J.J. Lewandowski, A.L. Greer, Acta Mater. 60 (2012) 4800.
[39] Z.Q. Liu, W.H. Wang, M.Q. Jiang, Z.F. Zhang, Philos. Mag. Lett. 94 (2014) 658.
[40] W.L. Johnson, K. Samwer, Phys. Rev. Lett. 95 (2005) 195501.
[41] F. Jiang, Z.B. Zhang, L. He, J. Sun, H. Zhang, Z.F. Zhang, J. Mater. Res. 21 (2006) 2638.
[42] A. Slipenyuk, J. Eckert, Scr. Mater. 50 (2004) 39.
[43] W.F. Wu, Y. Li, C.A. Schuh, Philos. Mag. 88 (2008) 71.
[44] Z.F. Zhang, J. Eckert, L. Schultz, Acta Mater. 51 (2003) 1167.
[45] A. Inoue, T. Zhang, T. Masumoto, J. Non-Cryst. Solids 156 (1993) 598.
[46] F.F. Wu, Z.F. Zhang, S.X. Mao, Acta Mater. 57 (2009) 257.
[47] R.T. Qu, M. Stoica, J. Eckert, Z.F. Zhang, J. Appl. Phys. 108 (2010) 063509.
[48] X.K. Xi, D.Q. Zhao, M.X. Pan, W.H. Wang, Y. Wu, J.J. Lewandowski, Phys. Rev. Lett. 94 (2005) 125510.
[49] M.Q. Jiang, Z. Ling, J.X. Meng, L.H. Dai, Philos. Mag. 88 (2008) 407.
[50] G. Wang, D.Q. Zhao, H.Y. Bai, M.X. Pan, A.L. Xia, B.S. Han, X.K. Xi, Y. Wu, W.H. Wang, Phys. Rev. Lett. 98 (2007) 235501.
[51] J.X. Zhao, R.T. Qu, F.F. Wu, Z.F. Zhang, B.L. Shen, M. Stoica, J. Eckert, J. Appl. Phys. 105 (2009) 103519.
[52] F.F. Wu, W. Zheng, S.D. Wu, Z.F. Zhang, J. Shen, Int. J. Plast. 27 (2011) 560.
[53] L.C. Zhang, F. Jiang, Y.L. Zhao, J.F. Zhang, L. He, J. Sun, Mater. Sci. Eng. A 527 (2010) 4122.
[54] Z.F. Zhang, F.F. Wu, G. He, J. Eckert, J. Mater. Sci. Technol. 23 (2007) 747.
[55] A. Christiansen, J.B. Shortall, J. Mater. Sci. 11 (1976) 1113.
[56] R.L. Narayan, P. Tandaiya, R. Narasimhan, U. Ramamurty, Acta Mater. 80 (2014) 407.
[57] P. Tandaiya, U. Ramamurty, R. Narasimhan, J. Mech. Phys. Solids 57 (2009) 1880.
[58] P. Tandaiya, R. Narasimhan, U. Ramamurty, Acta Mater. 61 (2013) 1558.
[59] Z.F. Zhang, J. Eckert, Phys. Rev. Lett. 94 (2005) 094301.
[60] P. Murali, T.F. Guo, Y.W. Zhang, R. Narasimhan, Y. Li, H.J. Gao, Phys. Rev. Lett. 107 (2011) 215501.
[61] X.X. Xia, W.H. Wang, Small 8 (2012) 1197.
[62] F. Spaepen, Acta Metall. 23 (1975) 615.
[63] A.S. Argon, M.S. Salama, Mater. Sci. Eng. 23 (1976) 219.
[64] J.P. Escobedo, Y.M. Gupta, J. Appl. Phys. 107 (2010) 123502.
[65] P.G. Debenedetti, F.H. Stillinger, Nature 410 (2001) 259.
[66] M.L. Falk, J.S. Langer, Phys. Rev. E 57 (1998) 7192.
[67] L.C. Zhang, F. Jiang, Y.L. Zhao, S.B. Pan, L. He, J. Sun, J. Mater. Res. 25 (2010) 283.